PeerJ

Artemisinin mimics calorie restriction to trigger mitochondrial biogenesis and compromise telomere shortening in mice

Da-Ting Wang[1,4], Jiang He[1,4], Ming Wu[2], Si-Ming Li[3], Qian Gao[1] and Qing-Ping Zeng[1]

[1] Tropical Medicine Institute, Guangzhou University of Chinese Medicine, Guangzhou, China
[2] School of Life Science, Sun Yat-sen University, Guangzhou, China
[3] The Second Affiliated Hospital, Guangzhou University of Chinese Medicine, Guangzhou, China
[4] These authors contributed equally to this work.

ABSTRACT

Calorie restriction is known to extend lifespan among organisms by a debating mechanism underlying nitric oxide-driven mitochondrial biogenesis. We report here that nitric oxide generators including artemisinin, sodium nitroprusside, and *L*-arginine mimics calorie restriction and resembles hydrogen peroxide to initiate the nitric oxide signaling cascades and elicit the global antioxidative responses in mice. The large quantities of antioxidant enzymes are correlated with the low levels of reactive oxygen species, which allow the down-regulation of tumor suppressors and accessory DNA repair partners, eventually leading to the compromise of telomere shortening. Accompanying with the up-regulation of signal transducers and respiratory chain signatures, mitochondrial biogenesis occurs with the elevation of adenosine triphosphate levels upon exposure of mouse skeletal muscles to the mimetics of calorie restriction. In conclusion, calorie restriction-triggered nitric oxide provides antioxidative protection and alleviates telomere attrition via mitochondrial biogenesis, thereby maintaining chromosomal stability and integrity, which are the hallmarks of longevity.

Subjects Biochemistry, Genomics, Pharmacology
Keywords Artemisinin, Calorie restriction, Nitric oxide, Hydrogen peroxide, BRCA1, Telomere

Submitted 30 October 2014
Accepted 16 February 2015
Published 5 March 2015

Corresponding author
Qing-Ping Zeng, qpzeng@163.com

Academic editor
Joao Rocha

Additional Information and Declarations can be found on page 20

DOI **10.7717/peerj.822**

INTRODUCTION

Calorie restriction (CR) is a robust and extensively reproducible intervention of lifespan extension among organisms ranging from yeast to mammals (*Koubova & Guarente, 2005*; *Spindler, 2010*). CR is supposed to exert a longevity-promoting effect through enhanced mitochondrial biogenesis, which is initiated by nitric oxide (NO) derived from endothelial nitric oxide synthase (eNOS) (*Nisoli et al., 2003*; *Nisoli et al., 2005*; *López-Lluch et al., 2006*). It is also noted that the increment of respiratory activity increases cell and animal longevity (*Lanza & Nair, 2010*). An 'uncoupling to survival' hypothesis suggests that CR may increase respiratory activity and extend life expectancy by uncoupling oxidation from phosphorylation (*Brand, 2000*). Indeed, several mitochondrial uncoupling strategies allow lifespan extension in yeast (*Barros et al., 2004*), nematodes (*Lemere et al., 2009*), and fruit flies (*Humpherey et al., 2009*). A low dose of the mitochondrial uncoupler 2,4-dinitrophenol (DNP) remarkably extends mouse lifespan (*Cerqueira, Laurindo & Kowaltowski, 2011*).

It is clear that DNP carries protons to leak across the inner mitochondrial membrane, leading to the disconnection of both adenosine triphosphate (ATP) regeneration from adenosine monophosphate (AMP) and oxidized nicotinamide adenine dinucleotide (NAD^+) conversion to reduced nicotinamide adenine dinucleotide ($NADH + H^+$) (*Korde et al., 2005*). The increases of AMP and NAD^+ can separately activate AMP-activated kinase (AMPK) and NAD^+-dependent deacetylase Sirtuin 1 (SIRT1), which can coordinately activate peroxisome proliferator-activated receptor-γ co-activator 1α (PGC-1α) essential for mitochondrial biogenesis (*Rodgers et al., 2005*; *Lee et al., 2006*). It has been recently demonstrated that the AMPK activator metformin mimics CR to improve healthspan and extend lifespan in mice (*Martin-Montalvo et al., 2013*). The SIRT1 activator resveratrol has been also known to exert CR-like beneficial effects on obese humans' life quality (*Blagosklonny, 2010*).

Since metabolic suppression was suggested to mitigate DNA damage (*Koubova & Guarente, 2005*), a novel model deciphering CR-conferred DNA protection has been established, in which CR-mediated metabolic/hormonal adaptations result in cellular adaptations including reduced cell proliferation, increased autophagy or apoptosis, up-regulated DNA repair systems, and enhanced genomic stability (*Longo & Fontana, 2010*). Most recently, CR has been shown to synergize with telomerase for promoting mouse longevity, suggesting a role of shortened telomeres in aging (*Vera et al., 2013*). Nevertheless, it has not yet been identified the mechanism by which CR protects DNA and telomeres.

According to the findings that CR induces NO (*Nisoli et al., 2003*; *Nisoli et al., 2005*) and NO competitively binds to cytochrome *c* oxidase (COX) (*Mason et al., 2006*), we propose here that CR-triggered NO might interact with COX to initiate mitochondrial uncoupling, which would provoke oxidative burst, activate antioxidative responses, mitigate DNA damage, and thereby compromise telomere shortening. To provide evidence supporting our proposition, we choose three different types of *in vivo* NO generators to replicate the effect of CR-triggered NO on the integrity of telomeres in mice. Artesunate (ART) is a semi-synthetic soluble derivative of artemisinin, a sesquiterpene endoperoxide that has been clinically used for antimalaria, and has been identified as an inhibitor of nitric oxide synthase (NOS) and an inducer of NO (*Zeng & Zhang, 2011*; *Zeng et al., 2011*). Sodium nitroprusside (SNP) as an NO donor and *L*-arginine (ARG) as an NO precursor have been widely used in modern medicine. Additionally, hydrogen peroxide (H_2O_2) was also included to simulate NO-posed oxidative stress that elicits antioxidative responses.

From the present study, we have disclosed the implication of NO signaling in telomere maintenance, and replayed the molecular episode of NO-mediated telomere protection. Also, we have rehearsed H_2O_2-compromised telomere shortening. In such context, we can explain why CR extends lifespan by annotating that CR triggers NO burst, initiates mitochondrial biogenesis, scavenges reactive oxygen species, attenuates DNA damage, and alleviates telomere attrition, thereby eventually leading to lifespan extension. We expect that the elucidation of *de novo* mechanisms underlying anti-aging/longevity in mammals should beneficial to a better solution to more and more severe human health issues.

MATERIALS AND METHODS

Animals and treatment procedures

Kunming (KM) mice, belonging to an outbred population originated from SWISS mice, were used in the present study. All mice were housed on a 12-h light: 12-h dark cycle at 25 °C, and fed with either *ad libitum* (AL) or 60% AL (CR). For treatment, AL mice were injected by 260 μM ART, 67 μM SNP, 5.7 mM ARG, or 200 μM H_2O_2 in 50 μl injection volume/20 g body weight. Each drug was injected into an identical loci of the skeletal muscles on one hind-leg, and samples were collected from skeletal muscle tissues around the injected sites. Animal procedures were in accordance with the animal care committee at the Guangzhou University of Chinese Medicine, Guangzhou, China. The protocol was approved by the Animal Care Welfare Committee of Guangzhou University of Chinese Medicine (Permit Number: SPF-2011007).

Enzyme-linked immunosorbent assay (ELISA)

All target proteins/peptides, including CAT, COX4, eNOS, GSH, SIRT3, SOD1, and SOD2, as well as the reference protein, glyceraldehyde-3-phosphate dehydrogenase (GAPDH), were immunoquantified according to antibody manufacture's manuals. The antibody against eNOS was purchased from Assay Biotechnology Co. Ltd. (Sunnyvale, CA, USA). The antibody against COX4 was purchased from Beijing Biosynthesis Biotechnology Co. Ltd. (Beijing, China). Other first antibodies were purchased from R & D Systems, Inc. ROS levels were measured with a Mouse ROS ELISA Kit (EIAab Science Co. Ltd., Wuhan, China) following the manufacturer's instructions.

Western blotting

The antibodies against AMPKα1/2 (H-300), AMPKα1/2 (Thr172), Akt1 (B-1), CYT C (H-104), PGC-1 (H-300), p-Akt1/2/3 (Ser473), and p-MFN2 (H-68) were purchased from Santa Cruz Biotechnology, Inc. (Dallas, Texas, USA). The SIRT1 antibody was purchased from Milipore (Temecula, California, USA). The eNOS antibody was purchased from Assay Biotechnology Co. Ltd. (Sunnyvale, CA, USA). The p-eNOS (Ser1177) antibody was purchased from Cell Signaling Technology, Inc. (Danvers, Massachusetts, USA). The blotting experiments were performed obeying to the manufacturer's instruction manuals. The gray scale values from blotted proteins were measured using a scanning instrument, and the raw data of gray scale values were normalized by a gray scale value of the reference protein GAPDH available from each group.

Southern blotting

Total DNA was extracted and digested by the restriction enzymes *Hinf* I and *Rsa* I. Southern blotting was performed by the hybridization of digested DNA with digoxin-labeled $(TTAGGG)_4$ probes according to the manufacturer's instructions. The lengths of telomere fragment bands on the gel were estimated by comparison with the base pairs of DNA standards.

Table 1 The primer sequences and fragment lengths of amplified genes.

Genes	Primers	Fragment lengths (bp)
GAPDH	F:5'GTTGTCTCCTGCGACTTCA3' R:5'GCCCCTCCTGTTATTATGG3'	293
BRCA2	F:5'AAGCCAAGCCACATAGCACAG3' R:5'ACTCCAGCCGAACCTTCAAAT3'	164
RB	F:5'AAATCATCGTCACTGCCTACAA3' R:5'AGGAATCCGTAAGGGTGAACT3'	236
MYC	F:5'GACTGTATGTGGAGCGGTTTCT3' R:5'GCTGTCGTTGAGCGGGTAG3'	213
RAD50	F:5'AGTTTACTCCCAGTTCATTACGC3' R:5'CTCTATTGACACTCTGTAGTCGGTT3'	287
RAD51	F:5'CTGCCCTTTACAGAACAGACTACTC3' R:5'GGCTACTACCTGGTTGGTGATTAC3'	140
TERT	F:5'GCCCAGACCTCAATTAAGACGA3' R:5'CTTCAACCGCAAGACCGACA3'	96

Quantitative polymerase chain reaction (qPCR)

Total RNA was extracted from mouse skeletal muscle cells by a Trizol methods. The primers with the sequences listed in Table 1 were synthesized by Invitrogen (Carlsbad, California, USA). The copy numbers of amplified genes were estimated by $2^{-\Delta\Delta Ct}$, in which $\Delta\Delta Ct =$ [target gene (treatment group)/target gene (control group)]/[house-keeping gene (treatment group)/house-keeping gene (control group)]. The raw qPCR data were normalized by the copy numbers of the reference gene *GAPDH*.

RT-PCR array

The Mouse Ubiquitylation Pathway RT^2 Profiler^{TM}PCR Array was provided by SABioscience Qiagen, (Hilden, Germany). The experiments were performed by Kangchen Biotechnology Co., Ltd., Shanghai, China.

Laser confocal microscopy

The fresh samples of mouse skeletal muscles were fixed in paraformadehyde for 24 h. After repeatedly rinsed, the fixed tissues were dehydrated by gradient ethanol. For embedding and sectioning, the tissue slices were pasted on the slides and coated at 50 °C. After they were dewaxed by a transparent reagent and rinsed, the slides were incubated with antibodies and stained by DAPI. After drying, a fluorescence quencher was added and slides were sealed. The fluorescence-labeled second antibodies and the first antibodies against BRCA1 and TERT were purchased from Beijing Biosynthesis Biotechnology Co., Ltd. (Beijing, China). Immunoblotting was carried out based on the manufacturer's instructions.

Electronic microscopy

After treatment, cells were harvested and fixed in 2.5% glutaraldehyde in 0.1 M phosphate buffer for three hours at 4 °C, followed by post-fixation in 1% osmium tetroxide for one

hour. Samples were dehydrated in a graded series of ethanol baths, and infiltrated and embedded in Spurr's low-viscosity medium. Ultra-thin sections of 60 nM were cut in a Leica microtome, double-stained with uranyl acetate and lead acetate, and examined in a Hitachi 7700 transmission electron microscope at an accelerating voltage of 60 kV.

Determination of NO and ATP levels

The NO and ATP levels were determined by the reagent kits manufactured by Jiancheng Biotechnology Institute, Nanjing, China. The NO levels (μM/g) $=(OD_{test} - OD_{blank})/(OD_{standard} - OD_{blank})$ • standard nitrate concentration (20 μM)/sample protein concentration (μg/μl). The ATP levels (μM/g) $=(OD_{test} - OD_{blank})/(OD_{standard} - OD_{blank})$ • standard ATP concentration (1000 μM) • sample dilution folds/sample protein concentration (μg/μl).

Statistical analysis

Statistical analyses were conducted by the one-way ANOVA method using SPSS version 17.0 for Windows. All data were represented as mean ± SEM unless otherwise stated. The XY graphs and column graphs were plotted and depicted using GraphPad Prism version 4.0.

RESULTS

CR and mimetics up-regulate eNOS and COX4 coordinately in a time-dependent manner

Considering that the up-regulation of mitochondrial genes is essential for CR-elicited mitochondrial biogenesis via NO signaling, we tried to validate whether CR might up-regulate the mitochondrial biomarker COX4 via enhanced eNOS expression. For this purpose, we determined the quantities of eNOS and COX4 in the skeletal muscles of mice exposed to CR or injected by ART, SNP, or ARG. Because NO-driven mitochondrial biogenesis was assumed to accompany with oxidative burst, we also used H_2O_2 to mimic CR's inducible effects on the expression of eNOS and COX4.

Like CR exposure for as long as three months, treatment of mice by ART, SNP, ARG, or H_2O_2 for one, three, six hours, or three days allows the gradual increases of both eNOS quantities (Fig. 1A) and COX4 quantities (Fig. 1B). To reach a level of significant difference from the control (AL mice), ARG needs only one hour, H_2O_2 needs three hours, SNP needs six hours, and ART needs even three days. Among groups, ARG treatment exhibits the largest quantities of eNOS and COX4, even larger than those upon exposure to CR. Interestingly, H_2O_2 treatment also induces larger quantities of COX4 and equal quantities of eNOS as compared with NO generators.

These results indicate that ART, SNP, ARG, or H_2O_2 can mimic CR to induce the enhanced expression of eNOS and COX4, implying that CR may affect mitochondrial structure and enhance mitochondrial function through the involvement of NO and H_2O_2. Because accompanying with NO-posed oxidative stress, CR and mimetics are anticipated to elicit antioxidative responses at least in mitochondria or even throughout whole cells.

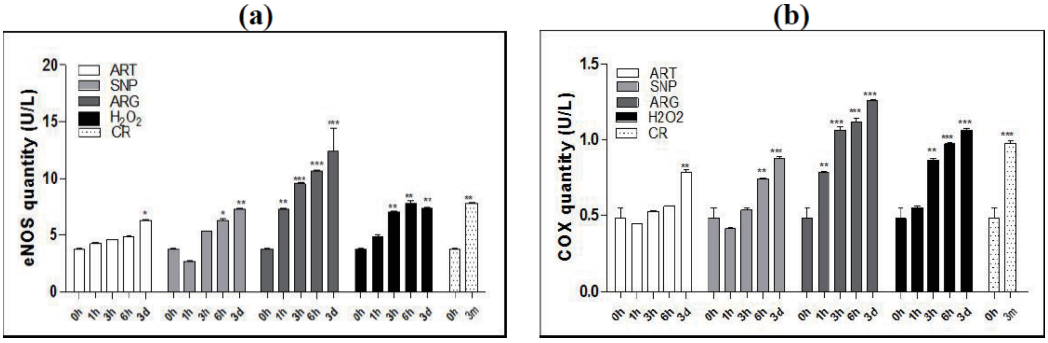

Figure 1 ART, SNP, ARG, or H_2O_2 mimics CR to increase the quantities of eNOS and COX4 in mouse skeletal muscle cells. (a) ELISA for eNOS measurement after treatment for different durations. (b) ELISA for COX4 measurement after treatment for different durations. 0 h represents AL; 3 m indicates CR for three months; and 1 h, 3 h, or 6 h means treatment for one hour, three hours, or six hours. ART (260 μM), SNP (67 μM), ARG (5.7 mM), or H_2O_2 (200 μM) was injected into the mouse skeletal muscle in the dose of 50 μl volume/20 g body weight. The 1 h, 3 h, or 6 h group had only one injection, and the 3d group had three daily injections. The ages of mice used are two-month-old except for CR mice, which are four-month-old with one-month AL and three-month CR treatment. The significance of statistical difference between a treatment sample and the AL sample was represented by * $P < 0.05$; ** $P < 0.01$; *** $P < 0.001 (n = 3)$.

CR and mimetics attenuate oxidative stress upon eliciting antioxidative responses

To reveal the effects of CR-triggered NO and H_2O_2 on the oxidative and antioxidative homeostasis, we monitored the dynamic changes of mitochondrial manganese superoxide dismutase (Mn-SOD, SOD2) and its activator SIRT3 in the skeletal muscle cells of mice treated by CR and mimetics. Consequently, both Mn-SOD (Fig. 2A) and SIRT3 (Fig. 2B) are synchronously up-regulated in a time-dependent manner after exposure to CR or injection by ART, SNP, ARG, or H_2O_2. While ARG induces the highest Mn-SOD quantity, SNP induces the highest SIRT3 quantity. These results demonstrate that antioxidation against oxidation is initiated from the activation of SIRT3-SOD2 in mitochondria of skeletal muscle cells after treatment of mice by CR and mimetics.

Except for specifically up-regulating Mn-SOD, CR and mimetics were also found to increase the quantities of total SOD enzymes that include cytosolic copper/zinc SOD (Cu/Zn-SOD, SOD1) (Fig. 2C). Additionally, CR and mimetics-treated mice exhibit the increases of catalase (CAT) and glutathione (GSH) (Figs. 2D and 2E), among which ARG induces the highest levels of SOD and GSH, while H_2O_2 induces the highest level of CAT. These results indicate that CR and mimetics can coordinately activate the antioxidative network in skeletal muscle cells, at least including SOD, CAT, and GSH.

Accordingly, a significant decline of the total levels of reactive oxygen species (ROS) in mouse skeletal muscle cells was observed after treatment of mice by ART, SNP, ARG, H_2O_2, or CR (Fig. 2F), suggesting an essential consequence of ROS scavenging by activated antioxidant enzymes. After treatment of mice by CR mimetics for one hour, SNP renders the lowest ROS level, H_2O_2 confers the second lower ROS level, and ARG and ART keeps a relatively lower ROS level than AL.

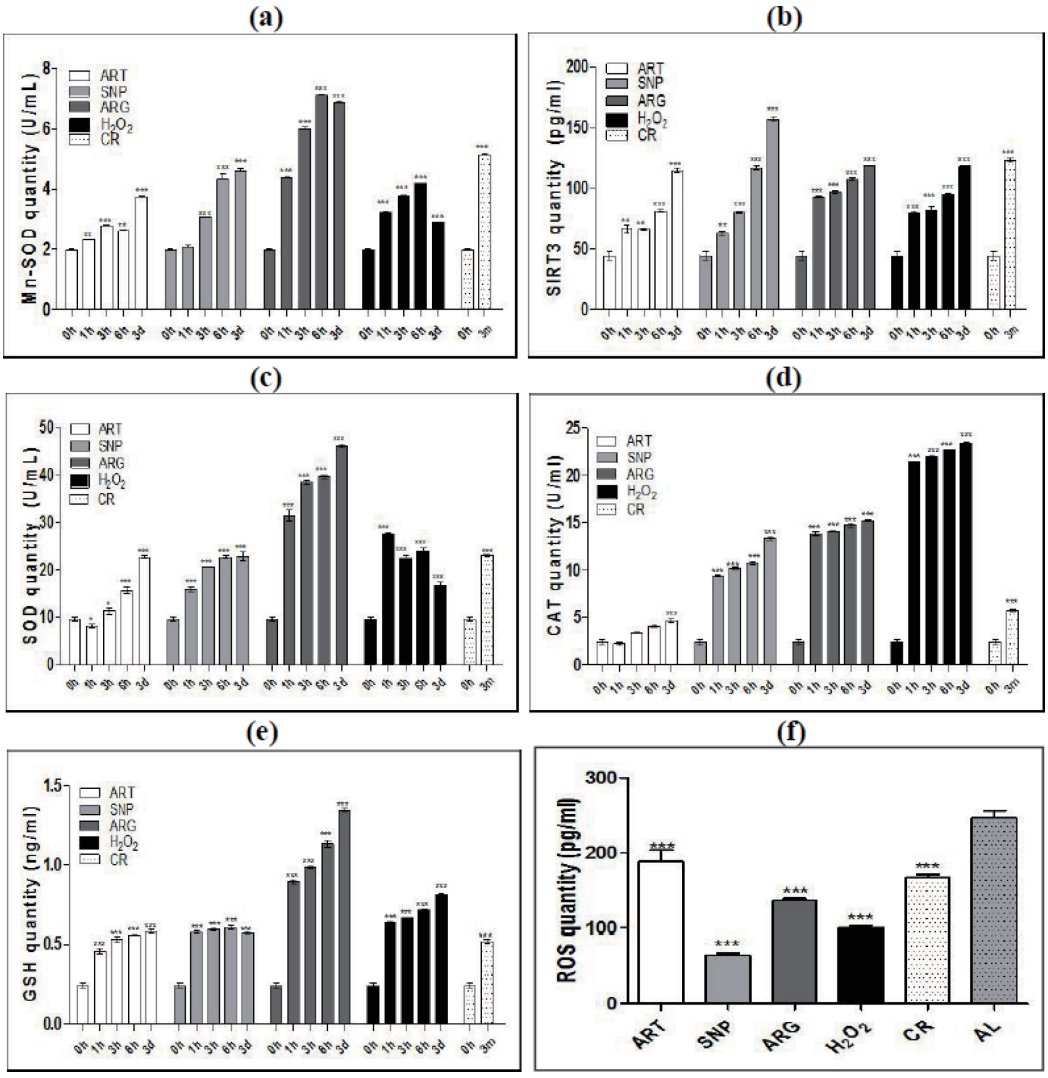

Figure 2 ART, SNP, ARG, H_2O_2, or CR activates antioxidant networks for ROS scavenging. (A) and (B) ELISA measurement of time-dependently induced mitochondria-localized Mn-SOD and SIRT3 by CR and mimetics. (C), (D), and (E) ELISA measurement of time-dependently induced SOD, CAT, and GSH by CR and mimetics. (F) ELISA measurement of the total ROS level in mice treated by CR and mimetics. 0 h represents AL; 3 m indicates CR for three months; and 1 h, 3 h, or 6 h means treatment for one hour, three hours, or six hours. ART (260 μM), SNP (67 μM), ARG (5.7 mM), or H_2O_2 (200 μM) was injected into the mouse skeletal muscle in the dose of 50 μl volume/20 g body weight. The 1 h, 3 h, or 6 h group had only one injection, and the 3d group had three daily injections. The ages of mice used are two-month-old except for CR mice, which are four-month-old with one-month AL and three-month CR treatment. The significance of statistical difference between a treatment sample and the AL sample was represented by * $P < 0.05$; ** $P < 0.01$; *** $P < 0.001$ ($n = 3$).

These results demonstrate that CR and mimetics can effectively stimulate the antioxidative responses in mouse skeletal muscle cells to quench ROS and create a less oxidative stress milieu.

CR and mimetics mostly down-regulate ubiquitylation pathway genes including tumor suppressors responsible for DNA repair

To make sure the relevance of CR and mimetics to the ubiquitin-mediated proteolysis pathway (UMPP) that is involved in the auto-regulated degradation of proteins, we set out to investigate whether CR and mimetics would affect the expression of ubiquitylation pathway genes. From the transcript profiling of ubiquitylation genes among ART, SNP, ARG, H_2O_2, and CR groups, it was noted that all 84 ubiquitylation genes examined are mostly down-regulated (Fig. 3, and see also Tables S1–S5 for details).

Among examined genes, 11 genes encoding ubiquitin-activating enzyme (E1) are unchanged or down-regulated in different groups, whereas 73 genes encoding ubiquitin-conjugating enzyme (E2) and ubiquitin-protein ligase (E3) genes are mostly down-regulated at a different extent. For example, one of the autophagy genes, *ATG7* (E1), is down-regulated for 35 folds in CR and for 2–5 folds in other treatment groups, and *UBE2C* (E2/E3) is down-regulated for 112 folds in CR and for 16–45 folds in other treatment groups. These results suggest that ubiquitylation-tuned protein degradation has been compromised upon exposure to CR for three months or after treatment by CR mimetics for three days.

The analysis of RT-PCR array data also indicates that a few of tumor suppressors and some DNA repair proteins are down-regulated, in which *BRCA1* is down-regulated for approximately 25 folds among all treatment groups, while *BARD1* is down-regulated for 30–60 folds by ART, SNP, or ARG, and five folds by CR. *TRP53* is slightly down-regulated in all treatment groups. Furthermore, we also detected the down-regulation of some BRCA1 partner-encoding genes including *BRCA2*, *MYC*, *RAD50*, and *RAD51* in CR mice. While *RB* is unchanged in CR mice, *MYC* and *RB* are mildly up-regulated by ART and H_2O_2. Besides, we observed that telomerase reverse transcriptase gene (*TERT*) is down-regulated by ARG, CR, and SNP, and unchanged after treatment by ART and H_2O_2 (Table 2).

From the fact that DNA repair genes are mostly down-regulated by CR and mimetics, we conclude that DNA damage in mice treated by CR and mimetics should be attenuated in a low oxidative milieu that is resulted from antioxidative activation and ROS scavenging. It is also conclusive that because oxidative DNA lesions are mitigated, *TERT* is of course accordingly down-regulated or unchanged in all treatment groups.

CR and mimetics-maintained longer telomeres are correlated with suppressed oxidative circumstance

From the results regarding the global down-regulation of tumor suppressor genes and accessory DNA repair genes by CR and mimetics, it can be expected that mice treated by CR and mimetics should have longer telomeres. To confirm this deduction, we compared the lengths of telomere restriction fragments (TRFs) from the skeletal muscle cells of CR

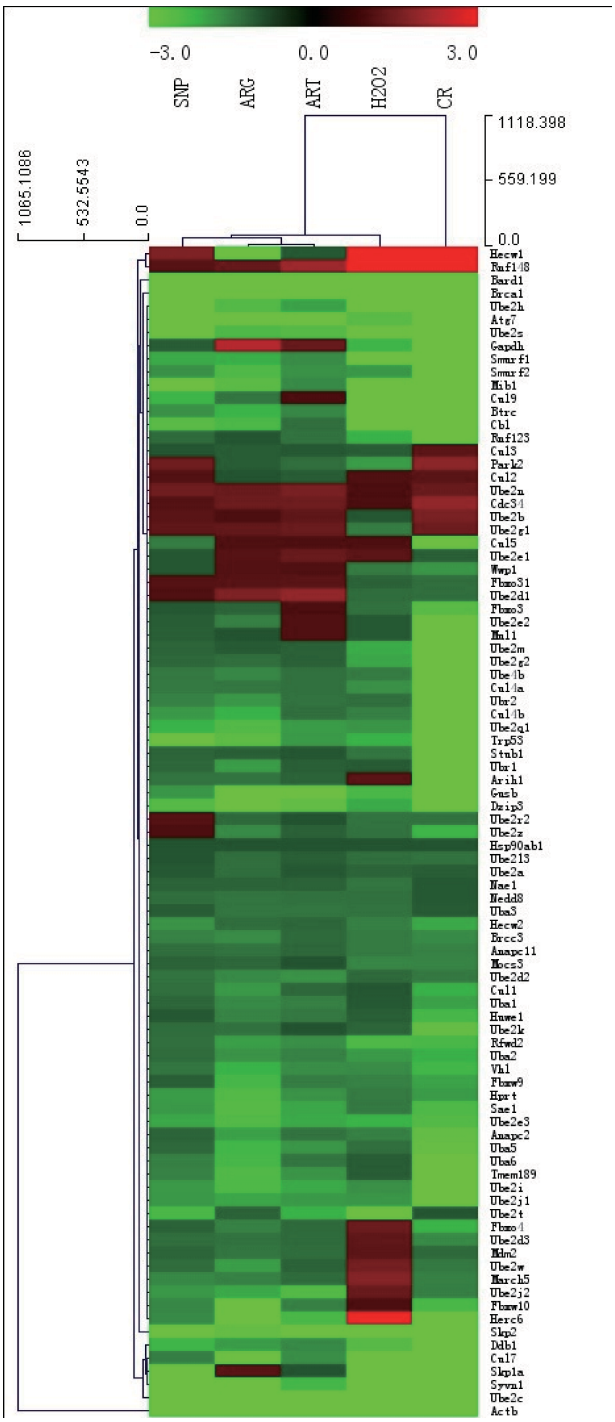

Figure 3 A hierarchical clustering illustration for the up/down-regulation of 84 ubiquitylation genes from RT-PCR array data. The red color represents up-regulation as compared with AL; and the green color represents down-regulation as compared with AL. The RT-PCR array was performed after daily injection for three days into mouse skeletal muscle by 260 μM ART, 67 μM SNP, 5.7 mM ARG in the dose of 50 μl volume/20 g body weight, or one injection by 200 μM H_2O_2 (50 μl/20 g), and sampling after last injection for six hours. The ages of all mice used are four-month-old, among which CR mice have one-month AL and three-month CR treatment.

Table 2 Quantification of amplified transcripts from DNA repair genes and TERT in skeletal muscle cells of mice treated by CR, H_2O_2, ART, SNP, ARG, or AL. (A) The normalization of quantified transcripts of DNA repair genes and TERT by a specific target gene vs the reference gene GAPDH. (B) The fold changes of quantified transcripts of DNA repair genes and TERT in treated mice vs AL mice.

Sample	BRCA2 /GAPDH	RB /GAPDH	MYC /GAPDH	RAD50 /GAPDH	RAD51 /GAPDH	TERT /GAPDH
CR	6.48E−05	3.21E−04	6.40E−05	3.33E−05	9.68E−05	1.64E−05
H_2O_2	9.87E−05	1.82E−03	4.62E−03	2.95E−04	1.39E−04	3.07E−05
ART	9.29E−05	1.48E−03	1.56E−03	5.79E−04	1.87E−04	4.14E−05
SNP	1.36E−04	1.64E−03	3.90E−04	3.31E−04	1.83E−04	1.94E−05
ARG	6.51E−05	1.17E−03	2.71E−04	3.02E−04	1.50E−04	7.36E−06
AL	1.13E−04	3.00E−04	2.83E−04	2.33E−04	1.29E−04	2.87E−05

Comparison	BRCA2 /GAPDH	RB /GAPDH	MYC /GAPDH	RAD50 /GAPDH	RAD51 /GAPDH	TERT /GAPDH
CR/AL	0.57	1.07	0.23	0.14	0.75	0.57
H_2O_2/AL	0.87	6.07	16.33	1.27	1.08	1.07
ART/AL	0.82	4.93	5.51	2.48	1.45	1.44
SNP/AL	1.20	5.47	1.38	1.42	1.42	0.68
ARG/AL	0.58	3.90	0.96	1.30	1.16	0.26

Notes.

The RT-PCR was performed after daily injection for three days into mouse skeletal muscle by 260 μM ART, 67 μM SNP, 5.7 mM ARG in the dose of 50 μl volume/20 g body weight, or one injection by 200 μM H_2O_2 (50 μl/20 g), and sampling after last injection for six hours. The ages of all mice used are four-month-old, among which CR mice have one-month AL and three-month CR treatment.

and mimetics-treated mice to those of an AL mouse. Consequently, TRFs of an AL sample were found to shift faster than those of ART, SNP, ARG, H_2O_2, and CR samples on the gel, suggesting AL TRFs being shorter than ART, SNP, ARG, H_2O_2, and CR TRFs (Fig. 4).

For more accurate comparison of TRFs among groups, we further measured the main band lengths, the longest band lengths, and the shortest band lengths of TRFs, and accounted for their average band lengths, as listed in Table 3. It is clear that SNP and H_2O_2 render longer average band lengths, whereas AL and CR confer shorter average band lengths. The main band lengths can be sorted as SNP > H_2O_2 > ARG > ART > CR > AL, and the longest band lengths are in the order of SNP > CR/H_2O_2 > ARG > AL > ART.

Interestingly, SNP and H_2O_2 lead to the lowest ROS levels (see Fig. 2F), which may partly decipher why SNP and H_2O_2 allow longer telomeres because longer telomeres are correlated with few ROS and less DNA damage. In contrast, AL and CR show the higher levels of ROS (see also Fig. 2F), thus providing an explanation on the relevance of more ROS to shorter telomeres. Why does CR give rise to the shortest TRFs than CR mimetics and even AL? This is likely due to the older ages of CR mice because they were older than other mice by three months when the telomere lengths were measured. As to the reason why younger mice were chosen for treatment by CR mimetics, we consider that the shortened telomeres in older mice should not be extended by CR mimetics.

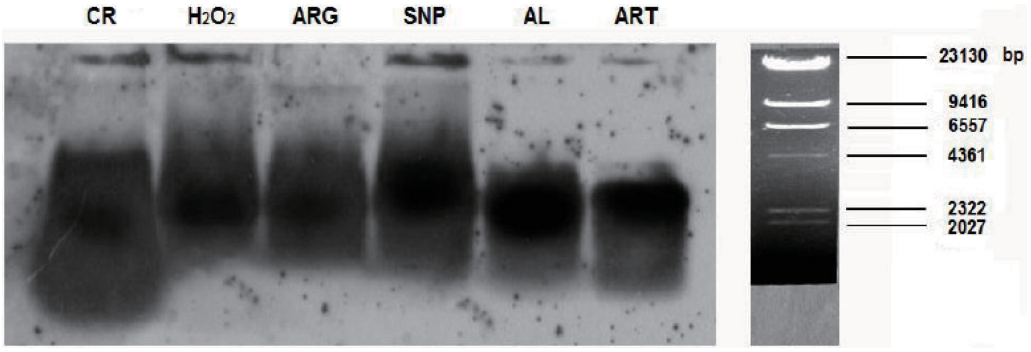

Figure 4 Hybridization detection of TRFs in mouse skeletal muscle cells of AL, CR and mimetics-treated mice. For Southern blotting, samples were collected from the skeletal muscle of AL and CR mice, or from CR mimetics mice injected by 260 μM ART, 67 μM SNP, 5.7 mM ARG, or 200 μM H_2O_2 in the dose of 50 μl volume/20 g body weight for three times, in which the 1st, 2nd, and 3rd injections are on the 1st, 3rd, and 5th day, respectively. The ages of AL and CR mimetics-treated mice are two-month-old, and the ages of CR mice are five-month-old, including one-month AL and four-month CR treatment.

Table 3 Measurement of TRF lengths in mouse skeletal muscle cells among AL, CR, and CR mimetics groups.

Group	The main band length (bp)	The longest band length (bp)	The shortest band length (bp)	The average band length (bp) ($\bar{x} \pm s$)
AL	2353	3077	1592	2341 ± 743
ART	2450	2956	2058	2488 ± 450
SNP	2917	3917	1717	2850 ± 1102
ARG	2551	3566	1476	2531 ± 1045
H_2O_2	2691	3814	1717	2741 ± 1049
CR	2450	3814	1142	2469 ± 1336

Notes.

For TRF measurement, samples were collected from the skeletal muscles of AL and CR mice, or from CR mimetics mice injected by 260 μM ART, 67 μM SNP, 5.7 mM ARG, or 200 μM H_2O_2 in the dose of 50 μl volume/20 g body weight for three times every other day. The ages of AL and CR mimetics mice are two-month-old, but the ages of CR mice are five-month-old, including one-month AL treatment and four-month CR treatment.

Co-existence of BRCA1 and TERT in similar abundance in nuclei implies an interaction of BRCA1 with TERT

As described above, *BRCA1* and *TERT* are down-regulated at the level of transcription (the mRNA level) (see Fig. 3 and Table 2). To ensure if BRCA1 and TERT are also down-regulated at the level of translation (the protein level), we tried to phenotyping the localization of BRCA1 and TERT in the skeletal muscle cells of AL, CR, and CR mimetics-treated mice. As a consequence, TERT was shown to co-exist with BRCA1 in overlapped nuclear locations, which can be clearly observed from the AL sample (Fig. 5), suggesting that TERT and BRCA1 may be interactive and cooperative. As to the dimmed BRCA1-TERT signals in ART, SNP, and ARG samples, they might represent the dual down-regulation of BRCA1 and TERT.

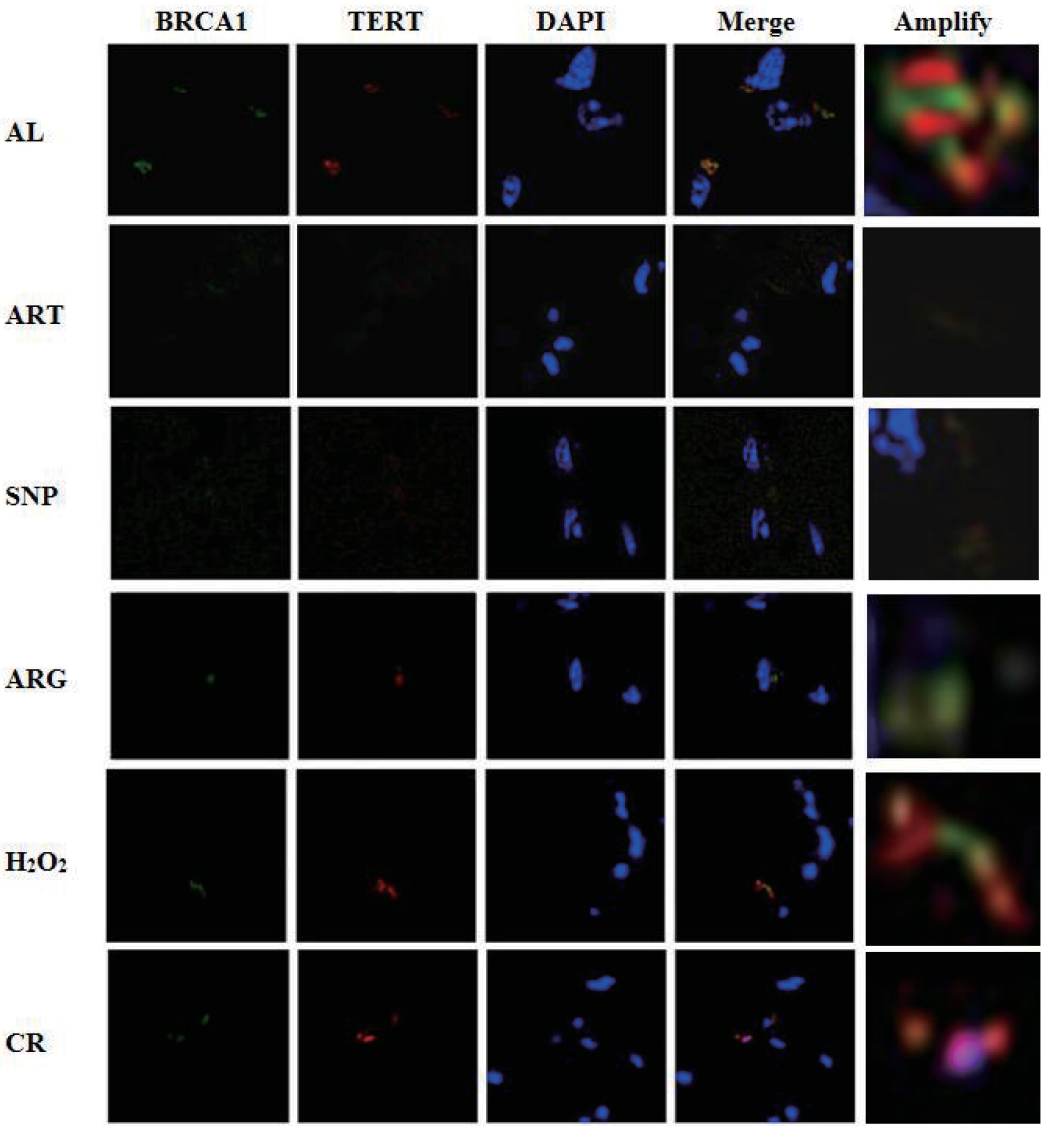

Figure 5 Laser confocal microscopic phenotyping of coordinated down-regulation of BRCA1 with TERT in mouse skeletal muscles treated by ART, SNP, ARG, H_2O_2, or CR. Green fluorescence indicates BRCA1, red fluorescence indicates TERT, and blue fluorescence represents 4',6-diamidino-2-phenylindole (DAPI)-staining nuclear DNA. For observation by a laser confocal microscope, samples were collected from the skeletal muscles of mice injected by 260 μM ART, 67 μM SNP, 5.7 mM ARG or 200 μM H_2O_2 (50 μl/20 g) for three times, in which the 2nd and the 3rd injections are on the 3rd and 5th day, respectively. The ages of AL and CR mimetic mice are two-month-old, but the ages of CR mice are five-month-old, including one-month AL treatment and four-month CR treatment.

Because the fluorescence strengths of TERT and BRCA1 are almost identical in each group albeit with lighter or darker fluorescence due to up- or down-regulation, we assume that both DNA-maintaining proteins perhaps accumulate with similar abundance, which is likely tuned by oxidative-antioxidative homeostasis.

ART, SNP, or ARG up-regulates eNOS, upstream protein kinases, and downstream respiratory biomarkers

To ascertain the possibility of ART, SNP, or ARG mediating NO signaling, we evaluated the expression and phosphorylation of eNOS and its upstream protein kinases, including Akt and AMPK. As results, their non-phosphorylated/phosphorylated forms, AMPK and p-AMPK^{Thr172}, Akt and p-Akt^{Ser473}, and eNOS and p-eNOS^{Ser1177}, are simultaneously induced in the skeletal muscle cells of mice injected by ART, SNP, or ARG (Fig. 6A and Table 4). AMPK and p-AMPK^{Thr172} exhibit almost identical expression levels, suggesting a synchronous mode of AMPK expression and phosphorylation. Akt and eNOS show higher levels than p-Akt^{Ser473} and p-eNOS^{Ser1177}, implying only a minor of Akt and eNOS being phosphorylated. These results indicate that ART, SNP, or ARG can synchronously induce eNOS, Akt, and AMPK, and partially activate them into p-eNOS^{Ser1177}, p-Akt^{Ser473}, and p-AMPK^{Thr172}.

To reinforce the relevance of NO-induced gene expression to mitochondrial biogenesis, we quantified some related signal transducers and mitochondria-targeted proteins in mouse skeletal muscles injected by ART, SNP, or ARG. Consequently, it was found that ART, SNP, or ARG leads to the significant up-regulation of the signaling components, SIRT1 and PGC-1α, and mitochondrial biomarkers, MFN2 and CYT C. As noted, PGC-1α shows the highest expression level, and SIRT1 also exhibits a mildly induced level (Fig. 6B and Table 4). These results indicate that NO can up-regulate the mitochondria-localized MFN2 and CYT C through inducing the mitochondrial biogenesis-necessitated SIRT1 and PGC-1α.

To understand the sequential events occurring in NO signaling and mitochondrial biogenesis, we followed up the time-course changes of selective signal transducers and mitochondrial biomarkers. In monitoring the expression of AMPK, PGC-1α, and CYT C in mouse skeletal muscles injected by ART, SNP, or ARG for three, six, and 24 h, we observed that AMPK reaches its maximal level within three hours and subsequently maintains a stable-steady level. PGC-1α and CYT C also exhibit the time-dependent expression manners, namely the three hour-treatment allows only the lower levels, the six hour-treatment leads to the elevated levels, and the 24 h-treatment gives rise to the highest levels. Importantly, the 24 h-expression level of PGC-1α is higher than that of CYT C (Fig. 6C and Table 4). These results demonstrate that the induction of understudied genes occurs in the sequelae from AMPK to PGC-1α and CYT C rather than *vice versa*.

CR mimetics-derived high-level NO predisposes mitochondrial biogenesis in mouse skeletal muscle cells

The ELISA and Western blotting data have revealed the induced up-regulation of eNOS by CR mimetics, but direct evidence confirming the elevation of NO levels is still lacking.

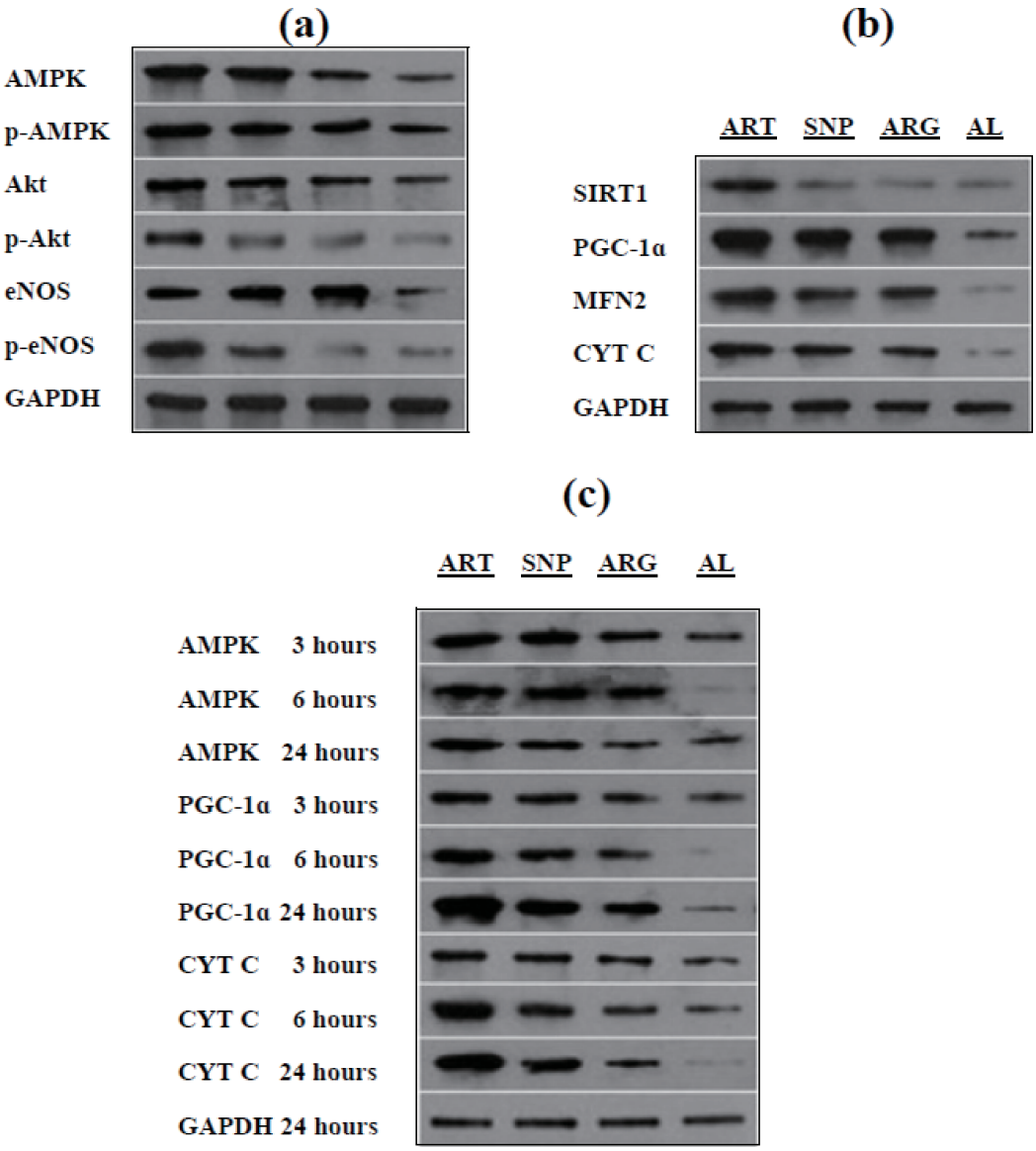

Figure 6 Western blotting of target proteins in mouse skeletal muscles injected by ART, SNP, or ARG. (A) Up-regulation and phosphorylation of eNOS and upstream protein kinases. (B) Up-regulation of mitochondrial biomarkers and relevant signal transducers. (C) The time-course mode of up-regulation of signal transducers and mitochondrial biomarkers. Western blotting was performed after three days of daily injection by 260 μM ART, 67 μM SNP, or 5.7 mM ARG (50 μl volume/20 g body weight). For each group of blots, only one stripe of gel with GAPDH bands was shown as reference, but blotting of each target protein was parallelly performed with GAPDH for comparison.

We monitored the NO levels in skeletal muscles of mice injected by ART, SNP, ARG, or H_2O_2. A NO burst was seen after treatment for six hours although a decline trend was observed after treatment for three days (Fig. 7A), addressing that all kinds of CR mimetics used in this study play their roles upon NO signaling. Furthermore, we also measured the ATP levels in the skeletal muscles of mice injected by ART, SNP, ARG, or H_2O_2. The results as depicted in Fig. 7B indicate that ATP is increased after treatment for six hours, but

Table 4 The time-course monitoring of expression levels of eNOS and upstream/downstream target proteins in the skeletal muscle cells of mice treated by ART, SNP, or ARG. (A) The gray scale values for target proteins to the reference protein GAPDH. (B) The fold changes of gray scale values for target proteins in treated mice to AL mice.

Target/reference protein	ART	SNP	ARG	AL
AMPK/GAPDH	1.01 ± 0.01*	0.97 ± 0.23**	0.85 ± 0.08*	0.61 ± 0.09
p-AMPK/GAPDH	1.00 ± 0.02**	0.93 ± 0.04*	0.93 ± 0.01*	0.83 ± 0.01
Akt/GAPDH	0.97 ± 0.01**	0.95 ± 0.02**	0.62 ± 0.08*	0.31 ± 0.06
p-Akt/GAPDH	0.56 ± 0.40	0.21 ± 0.11	0.13 ± 0.11	0.09 ± 0.08
eNOS/GAPDH	0.93 ± 0.10***	0.94 ± 0.01***	0.97 ± 0.02***	0.15 ± 0.01
p-eNOS/GAPDH	0.86 ± 0.11*	0.53 ± 0.37	0.21 ± 0.06	0.19 ± 0.16
SIRT1/GAPDH	1.01 ± 0.05**	0.90 ± 0.03**	0.80 ± 0.05*	0.62 ± 0.04
PGC-1α/GAPDH	1.04 ± 0.63**	1.00 ± 0.04**	0.99 ± 0.05**	0.26 ± 0.16
MFN2/GAPDH	0.93 ± 0.02	0.58 ± 0.38	0.68 ± 0.03	0.32 ± 0.24
CYT C/GAPDH	0.94 ± 0.01**	0.67 ± 0.18*	0.50 ± 0.41*	0.11 ± 0.04
3 h AMPK/GAPDH	1.27 ± 0.05	1.24 ± 0.05	1.09 ± 0.05	0.77 ± 0.27
6 h AMPK/GAPDH	1.05 ± 0.22	0.95 ± 0.27	0.93 ± 0.31	0.68 ± 0.14
24 h AMPK/GAPDH	1.05 ± 0.27	1.06 ± 0.12	0.85 ± 0.04	0.69 ± 0.12
3 h PGC-1α/GAPDH	1.07 ± 0.03**	0.94 ± 0.06*	0.90 ± 0.02*	0.75 ± 0.03
6 h PGC-1α/GAPDH	0.79 ± 0.14*	0.75 ± 0.01	0.58 ± 0.01	0.34 ± 0.15
24 h PGC-1α/GAPDH	1.30 ± 0.07**	1.16 ± 0.03**	1.06 ± 0.07	0.58 ± 0.11
3 h CYT C/GAPDH	1.13 ± 0.02*	0.95 ± 0.02	0.93 ± 0.17	0.76 ± 0.02
6 h CYT C/GAPDH	1.29 ± 0.04**	1.01 ± 0.07*	0.97 ± 0.17*	0.64 ± 0.03
24 h CYT C/GAPDH	1.40 ± 0.03**	1.25 ± 0.05**	0.71 ± 0.22	0.53 ± 0.06

Treated mice/AL mice	ART/AL	SNP/AL	ARG/AL
AMPK/GAPDH	1.66	1.59	1.39
p-AMPK/GAPDH	1.20	1.12	1.12
Akt/GAPDH	3.13	3.06	2.00
p-Akt/GAPDH	6.22	2.33	1.44
eNOS/GAPDH	6.20	6.27	6.47
p-eNOS/GAPDH	4.53	2.79	1.11
SIRT1/GAPDH	1.63	1.45	1.29
PGC-1α/GAPDH	4.00	3.85	3.81
MFN2/GAPDH	2.91	1.81	2.13
CYT C/GAPDH	8.55	6.09	4.55
3 h AMPK/GAPDH	1.65	1.61	1.42
6 h AMPK/GAPDH	1.54	1.40	1.37
24 h AMPK/GAPDH	1.52	1.54	1.23
3 h PGC-1α/GAPDH	1.43	1.25	1.20
6 h PGC-1α/GAPDH	2.32	2.21	1.71
24 h PGC-1α/GAPDH	2.24	2.00	1.83

(*continued on next page*)

Table 4 (*continued*)

Treated mice/AL mice	ART/AL	SNP/AL	ARG/AL
3 h CYT C/GAPDH	1.49	1.25	1.22
6 h CYT C/GAPDH	2.02	1.58	1.52
24 h CYT C/GAPDH	2.64	2.36	1.34

Notes.

Western blotting was performed after daily injection for three days by 260 μM ART, 67 μM SNP, or 5.7 mM ARG (50 μl volume/20 g body weight). GAPDH: glyceraldehyde-3-phosphate dehydrogenase. For each group of blots, only one stripe of gel with GAPDH bands was shown as reference, but blotting of each target protein was parallelly performed with GAPDH for comparison. The fold changes of gray scale values were calculated by comparing each target protein with corresponding GAPDH.

[*] The significance of statistical difference between a treatment sample and AL is represented by $P < 0.05$.

[**] The significance of statistical difference between a treatment sample and AL is represented by $P < 0.01$.

[***] The significance of statistical difference between a treatment sample and AL is represented by $P < 0.001$ ($n = 3$).

maintains a steady-state higher level after treatment for three days. These results provide support to the assumption of CR mimetics-enhanced mitochondrial functionality.

At last, we scrutinized whether the density of mitochondria would be changed in mouse skeletal muscle cells exposed to ART, SNP, ARG, or H_2O_2. As compared with one-layer and linear-arrayed mitochondria in AL-exposed cells (Fig. 7C), SNP-treated cells (Fig. 7D) or H_2O_2-treated cells (Fig. 7E) show remarkable mitochondrial proliferation with multi-layer mitochondria, and ART-treated cells (Fig. 7F) or ARG-treated cells (Fig. 7G) also possess more mitochondrial layers than AL-exposed cells after treatment for six hours.

These results unambiguously indicate that CR and mimetics can produce NO, drive mitochondrial biogenesis, and recover energy supply in mice during a short period, for example, within six hours as examined in the present study.

DISCUSSION

The mechanisms underlying CR-mediated lifespan extension have been eagerly and extensively investigated in recent years. A current research work in nematodes has well deciphered the reason why CR decreases ATP by reporting that increase of the citrate cycle intermediate α-ketoglutarate during CR exposure targets the subunit β of ATP synthase (complex V) and inhibits its activity, addressing an important role of mitochondrial uncoupling in prolonging lifespan (*Chin et al., 2014*). Although whether mitochondrial uncoupling correlates with redox homeostasis remains largely unknown, evidence is emerging to support the concept of mitochondrial hormesis (mitohormesis), which suggests that potent ROS burst from mitochondria evokes antioxidative responses and promotes life expectancy (*Ristow & Kim, 2010*; *Ristow, 2014*).

Indeed, mitochondrial superoxide production was found to increase the longevity of nematodes by triggering ROS-scavenging responses (*Yang & Hekimi, 2010*). It has been recently indicated that aspirin promotes mitochondrial biogenesis through H_2O_2 production and SIRT1/PGC-1α induction in cultured mouse liver cells (*Kamble et al., 2013*). A most new report has also demonstrated that H_2O_2 enables the up-regulation of mitochondria-specific SIRT3 and Mn-SOD in mice (*Qiu et al., 2010*). Following the finding of H_2O_2-mediated extension of yeast chronological lifespan through inducing

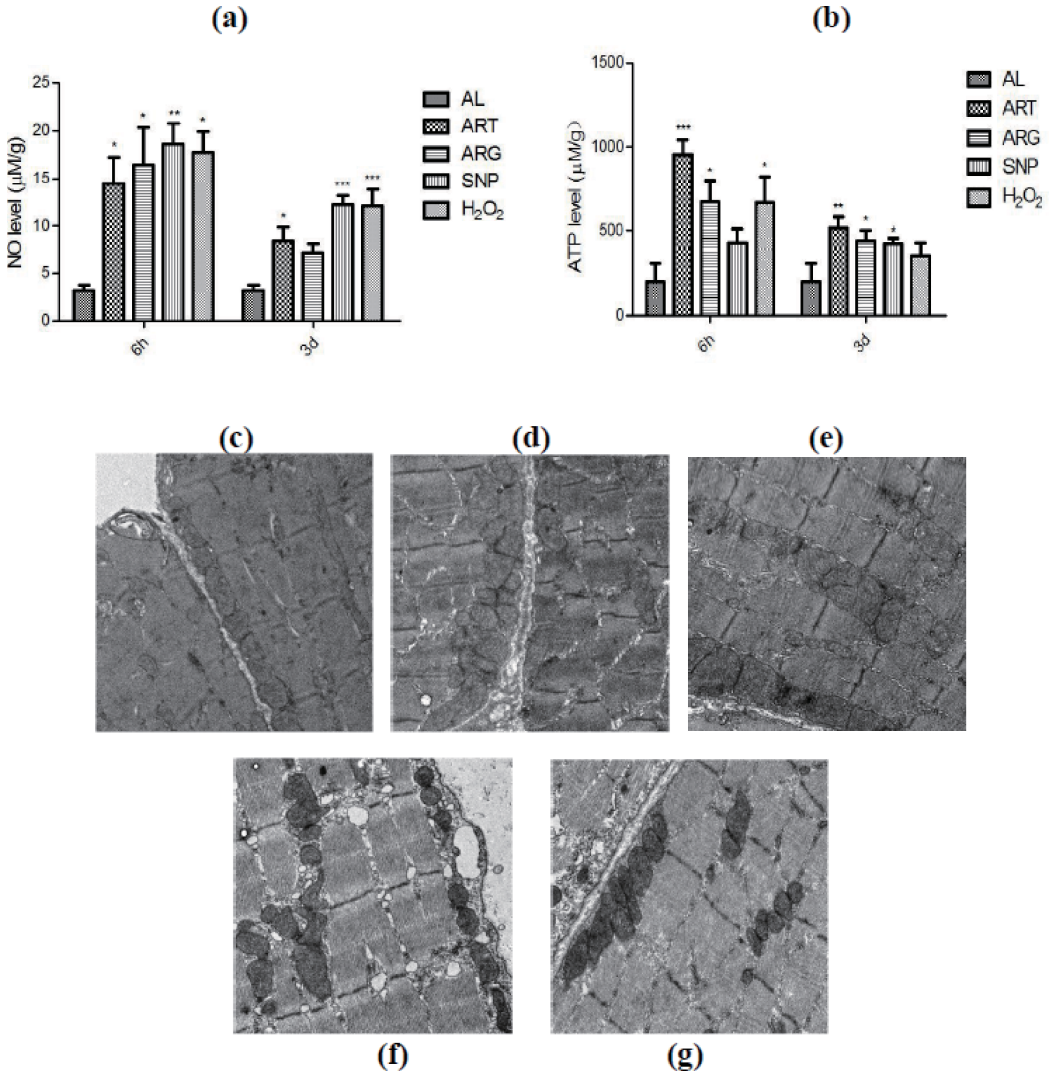

Figure 7 Determination of NO and ATP levels and electronic microscopic phenotyping of mitochondria in mouse skeletal muscles injected by ART, ARG, SNP, or H_2O_2. (A) The elevation of NO levels upon treatment by CR mimetics. (B) The elevation of ATP levels upon treatment by CR mimetics. (C)–(G) Mitochondrial density and structure in ART, ARG, SNP, H_2O_2, and AL, respectively. Samples were collected from mouse skeletal muscles after 6 h by one injection or by daily injection for three days by 260 μM ART, 67 μM SNP, 5.7 mM ARG, or 200 μM H_2O_2 (50 μl injection volume/20 g body weight).

antioxidative responses (*Mesquita et al., 2010*), we have also confirmed the mitohormetic effects of H_2O_2 on yeast chronological lifespan (*Wang & Zeng, 2014*). Most recently, metformin has been proven to promote lifespan in nematodes via the peroxiredoxin PRD-2-involved mitohormesis (*De Haes et al., 2014*).

In the present study, we found that ART, SNP, ARG, or H_2O_2 can mimic CR to induce SOD, CAT, and GSH, which lead to the alleviation of ROS-engaged stress. In particular, we observed the synchronous induction of mitochondrial SOD2 and its activator SIRT3 by CR and mimetics, which is in consistence with the known fact that CR dramatically reduces oxidative stress by inducing SIRT3-activated SOD2 (*Qiu et al., 2010*). Although it

is understandable that H_2O_2 as an oxidant enables the induction of antioxidant enzymes, why ART, SNP, and ARG also induce antioxidant enzymes seems puzzling. In our opinion, there may be two possibilities: one is the direct exertion by H_2O_2 generation, and another is indirect affection via NO production. It has been shown that H_2O_2 induces eNOS via a Ca_2^+/calmodulin-dependent protein kinase II/janus kinase 2-dependent pathway (*Cai et al., 2001*). We also found in this study that H_2O_2 not only up-regulates eNOS, but also produces NO, suggesting a plausible dependence of H_2O_2-induced antioxidation on NO signaling.

Nevertheless, how NO attenuates oxidative stress remains inclusive. It has been previously described that NO can non-covalently bind to COX, leading to the reversible COX inhibition and transient respiratory dysfunction (*Mason et al., 2006*). We assumed that an interaction of NO with COX should block electron transport, elicit ROS burst, and trigger antioxidative responses. Our quantification results of antioxidant enzyme quantities as well as the measurement data of ROS levels have altogether confirmed that CR and mimetics allow enhanced antioxidative ability and attenuated oxidative stress in mice. Another consequence of electron transport interruption is a short-term decrease of ATP due to mitochondrial uncoupling and a feedback increase of ATP upon mitochondrial biogenesis. Indeed, we detected the remarkable elevation of ATP levels in the skeletal muscles of mice treated by CR mimetics.

As to the debating issue of NO-mediated mitochondrial biogenesis, we also provided new supporting testimony by showing considerable mitochondrial propagation in the skeletal muscle cells of mice treated by CR mimetics. The discrepancy of findings that CR-mediated lifespan extension with or without mitochondrial biogenesis may be resulted from the earlier or later stages, in other words, an acute short-term or a chronic long-term CR. We have suggested a mechanistic model of dual-phase responses to CR exposure in yeast, in which the phase of mitochondrial enhancement within hours is a respiratory burst phase, and the phase of post-mitochondrial enhancement within days and months is a respiratory decay phase (*Wang et al., 2015*). It is reasonable that respiratory burst may be attributed to mitochondrial biogenesis, whereas respiratory decay should not be accompanied with mitochondrial biogenesis.

CR is evident to trigger NO production upon Akt-mediated eNOS activation in mice (*Nisoli et al., 2003*; *Nisoli et al., 2005*; *Cerqueira, Laurindo & Kowaltowski, 2011*). ARG is also shown to enhance eNOS expression (*Ou et al., 2010*), but how ART and SNP affect eNOS remains uncertain. We found in this study that ART, SNP, and ARG not only activate eNOS, but also produce NO, suggesting that they act as CR to initiate NO signaling in mice. A previous investigation has revealed that increase of the AMP/ATP ratio activates AMPK (*Anderson & Weindruch, 2010*). Earlier evidence has been filed that AMPK activates eNOS through the signaling cascade AMPK→ Rac1→ Akt→ eNOS (*Levine, Li & Michel, 2007*), in which AMPK and Akt are coordinately responsible for the activation of eNOS through the phosphorylation of Ser1177 (*Chen et al., 1999*; *Dimmeler et al., 1999*). Conclusively, ART, SNP, ARG, and H_2O_2 should activate eNOS along AMPK→ Rac1→ Akt→ eNOS.

Because SNP is an NO donor, and ARG is an NO precursor, it should be reasonable that SNP-released NO and ARG-produced NO *in vivo* can initiate NO signaling. However, ART neither releases NO as SNP, nor produces NO like ARG, so why would it also up-regulate eNOS? It has been indicated that ART alkylates the prosthetic heme of hemoproteins (*Zhang & Gerhard, 2009*). Our previous work has also shown that ART promotes NO generation by inhibiting the hemoprotein NOS via conjugating the heme moiety and inducing NOS expression either in human cell lines (*Zeng & Zhang, 2011*) or in bacteria (*Zeng et al., 2011*). Therefore, we anticipated that ART may interfere with the activity of the mitochondrial hemoprotein COX in direct and indirect ways: it may conjugate to the heme moiety of COX to repress its function; and it may also firstly conjugate to the heme moiety of eNOS to inhibit its activity, and secondly induce the overexpression of eNOS for NO generation and COX binding.

To verify those two possibilities, we should confirm the synchronous up-regulation of COX and eNOS upon induction by ART, thereby validating ART-COX and ART-eNOS interactions. As shown in our results, ART can simultaneously up-regulates eNOS and COX4, suggesting that the inhibition of eNOS and COX by ART may lead to the induction of *eNOS/NOS3* and *COX*expressions. Although the adducts of ART with hemoproteins were identified in human cell lines, bacteria, and yeast (*Zeng & Zhang, 2011*; *Zeng et al., 2011*; *Wang & Zeng, 2014*), we are at present unable to discriminate the ART-eNOS adducts from the ART-COX adducts or other ART-hemoprotein adducts.

It is worthy of indicating that low-dose ART is found, for the first time, to simulate the lifespan-prolonging effect. In regard to the dose-effect issue of ART, an earlier pharmacokinetical research indicated that when ART was administered at a dose of 6.7 mg/kg, a peak level of 0.82 μg/ml was attained in mice after four hours. This is a concentration more than 5000 times the IC_{50} of ART in the *in vitro* tests on *Plasmodium berghei* for antimalarial activity, and is also close to the human exposure that we see with clinical doses of ART (*Zhao et al., 1989*). Therefore, we used quite a low dose (50 μl 260 μM or 0.25 mg/kg) of ART for telomere protection in mice. We choose the dose of ART in the present study because we have previously used a similar dose of ART (100 μl 60 μg/ml or 0.3 mg/kg) for NOS induction and NO production in mice (*Bao et al., 2012*; *Wu et al., 2012*).

In this study, we noticed that CR or mimetics leads to the global down-regulation of many ubiquitylation pathway genes including DNA repair genes, such as BRCA1, BARD1, and TRP53, implying a cause-result relationship between rare DNA damage and less DNA repair. Furthermore, we also observed that some BRCA1 partners are down-regulated or unchanged in CR and mimetics-treated mice, strengthening a reverse relevance of DNA repair to DNA damage. BRCA1 is structurally identified to interact with other partner proteins for DNA repair (*Clark et al., 2012*), during which BRCA1 is recruited to the telomere and regulate telomere length and stability, in part through its presence at the telomere (*Ballal et al., 2009*). BRCA1 and BARD1 constitute a heterodimeric RING finger complex with ubiquitin ligase (E3) (*Hashizume et al., 2001*). A conclusion of repressed protein degradation is supported by the findings that CR significantly reduces age-related

impairments in proteasome-mediated protein degradation, and inhibits age-related increases in ubiquitinated, oxidized, and sumoylated proteins (*Li et al., 2008*).

Telomeres have been recently verified to be a favored target of persistent DNA damage in aging and stress-induced senescence (*Hewitt et al., 2012*), and a reverse correlation of BRCA1 with TERT has been previously established (*Xiong et al., 2003*), implying that the down-regulation of DNA repair genes is an important hint indicating attenuated DNA damage due to ROS scavenging by inducible antioxidation. Indeed, we detected longer telomeres in mouse skeletal muscle cells among treatment groups than those in AL mice. However, whether longer telomeres are due to compromised telomere shortening or enhanced telomere extension is unclear. Our preliminary results on the amplification of *TERT* mRNA show that it is unlikely up-regulated after underlying treatments. At the same time, we also observed the co-localization and overlap of BRCA1 and TERT with almost identical abundance, implying that TERT is synchronously fluctuated with BRCA1. Actually, we have testified the down-regulation of BRCA1 in RT-PCR array, so it is likely that longer telomeres are attributed to less DNA damage due to mitigated telomere shortening rather than more DNA repair leading to active telomere extension.

In conclusion, we revealed the mechanistic episodes of the effects of CR and mimetics on the dynamic changes of telomeres in mouse skeletal muscle cells. We also provide the direct information supporting the hormesis hypothesis by the validation of beneficial roles of CR mimetics on DNA protection. Therefore, our study should shed light on the discovery of new targets and development of new anti-aging drugs towards longevity.

ACKNOWLEDGEMENTS

We thank Kangchen Biotechnology Co, Shanghai, China for performance of RT-PCR array experiments. We also thank Ms. Zeng Weixia in Laura Biotechnology Co, Guangzhou, China for her technical assistance in TRF analysis.

ADDITIONAL INFORMATION AND DECLARATIONS

Funding

Financial support was provided by the National Science Foundation of China (NSFC). The funders had no role in study design, data collection and analysis, decision to publish, or preparation of the manuscript.

Grant Disclosures

The following grant information was disclosed by the authors:
National Science Foundation of China (NSFC).

Competing Interests

The authors declare there are no competing interests.

Author Contributions

- Da-Ting Wang performed the experiments, analyzed the data, contributed reagents/materials/analysis tools, prepared figures and/or tables, reviewed drafts of the paper.
- Jiang He performed the experiments.
- Ming Wu, Si-Ming Li and Qian Gao performed the experiments, reviewed drafts of the paper.
- Qing-Ping Zeng conceived and designed the experiments, analyzed the data, wrote the paper, prepared figures and/or tables, reviewed drafts of the paper.

Animal Ethics

The following information was supplied relating to ethical approvals (i.e., approving body and any reference numbers):

All animal procedures were in accordance with the animal care committee at the Guangzhou University of Chinese Medicine, Guangzhou, China. The protocol was approved by the Animal Care Welfare Committee of Guangzhou University of Chinese Medicine (Permit Number: SPF-2011007).

Microarray Data Deposition

The following information was supplied regarding the deposition of microarray data:

GEO: http://www.ncbi.nlm.nih.gov/geo/query/acc.cgi?acc=GSE65993.

Supplemental Information

Supplemental information for this article can be found online at http://dx.doi.org/10.7717/peerj.822#supplemental-information.

REFERENCES

Anderson RM, Weindruch R. 2010. Metabolic reprogramming, caloric restriction and aging. *Trends in Endocrinology and Metabolism* **21**:134–141 DOI 10.1016/j.tem.2009.11.005.

Ballal RD, Saha T, Fan S, Haddad BR, Rosen EM. 2009. BRCA1 localization to the telomere and its loss from the telomere in response to DNA damage. *Journal of Biological Chemistry* **284**:36083–36098 DOI 10.1074/jbc.M109.025825.

Bao F, Wu P, Xiao N, Qiu F, Zeng QP. 2012. Nitric oxide-driven hypoxia initiates synovial angiogenesis, hyperplasia and inflammatory lesions in mice. *PLoS ONE* **7**:e34494 DOI 10.1371/journal.pone.0034494.

Barros MH, Bandy B, Tahara EB, Kowaltowski AJ. 2004. Higher respiratory activity decreases mitochondrial reactive oxygen release and increases lifespan in *Saccharomyces cerevisiae*. *Journal of Biological Chemistry* **279**:49883–49888 DOI 10.1074/jbc.M408918200.

Blagosklonny MV. 2010. Linking calorie restriction to longevity through sirtuins and autophagy: any role for TOR. *Cell Death and Disease* **1**:e12 DOI 10.1038/cddis.2009.17.

Brand MD. 2000. Uncoupling to survive? The role of mitochondrial inefficiency in ageing. *Experimental Gerontology* **35**:811–820 DOI 10.1016/S0531-5565(00)00135-2.

Cai H, Davis ME, Drummond GR, Harrison DG. 2001. Induction of endothelial NO synthase by hydrogen peroxide via a Ca(2+)/calmodulin-dependent protein kinase II/janus kinase 2-dependent pathway. *Arteriosclerosis, Thrombosis, and Vascular Biology* **21**:1571–1576 DOI 10.1161/hq1001.097028.

Cerqueira FM, Laurindo FRM, Kowaltowski AJ. 2011. Mild mitochondrial uncoupling and calorie restriction increase fasting eNOS, AKT and mitochondrial biogenesis. *PLoS ONE* **6**:e18433 DOI 10.1371/journal.pone.0018433.

Chen ZP, Mitchelhill KI, Michell BJ, Stapleton D, Rodriguez-Crespo I, Witters LA, Power D, Oritz de Montellano PR, Kemp BE. 1999. AMP-activated protein kinase phosphorylation of endothelial NO synthase. *FEBS Letters* **443**:285–289 DOI 10.1016/S0014-5793(98)01705-0.

Chin RM, Fu X, Pai MY, Vergnes L, Hwang H, Deng G, Diep S, Lomenick B, Meli VS, Monsalve GC, Hu E, Whelan SA, Wang JX, Jung G, Solis GM, Fazlollahi F, Kaweeteerawat C, Quach A, Nili M, Krall AS, Godwin HA, Chang HR, Faull KF, Guo F, Jiang M, Trauger SA, Saghatelian A, Braas D, Christofk HR, Clarke CF, Teitell MA, Petrascheck M, Reue K, Jung ME, Frand AR, Huang J. 2014. The metabolite α-ketoglutarate extends lifespan by inhibiting ATP synthase and TOR. *Nature* **510**:397–401 DOI 10.1038/nature13264.

Clark SL, Rodriguez AM, Snyder RR, Hankins GD, Boehning D. 2012. Structure-function of the tumor suppressor BRCA1. *Computational and Structural Biotechnology Journal* **1**:e201204005 DOI 10.5936/csbj.201204005.

De Haes W, Frooninck XL, Van Assche R, Smolders A, Depuydet G, Billen J, Braeckman BP, Schoofs L, Temmerman L. 2014. Metformin promotes lifespan through mitohormesis via the peroxiredoxin PRDX-2. *Proceedings of the National Academy of Sciences of the United States of America* **111**:E2501–E2509 DOI 10.1073/pnas.1321776111.

Dimmeler S, Fleming I, Fisslthaler B, Hermann C, Busse R, Zeiher AM. 1999. Regulation of endothelium-derived nitric oxide production by the protein kinase AKT. *Nature* **399**:597–601 DOI 10.1038/21218.

Hashizume R, Fukuda M, Maeda I, Nishikawa H, Oyake D, Yabuki Y, Ogataand H, Ohta T. 2001. The RING heterodimer BRCA1–BARD1 is a ubiquitin ligase inactivated by a breast cancer-derived mutation. *Journal of Biological Chemistry* **276**:14537–14540 DOI 10.1074/jbc.C000881200.

Hewitt G, Jurk D, Marques FDM, Correia-Melo C, Hardy T, Gackowska A, Anderson R, Taschuk M, Mann J, Passos JF. 2012. Telomeres are favoured targets of a persistent DNA damage response in ageing and stress-induced senescence. *Nature Communications* **3**:Article 708 DOI 10.1038/ncomms1708.

Humpherey DM, Toivonen JM, Giannakou M, Partridge L, Brand MD. 2009. Expression of human uncoupling protein-3 in Drosophila insulin-producing cells increases insulin-like peptide (DILP) levels and shortens lifespan. *Experimental Gerontology* **44**:316–327 DOI 10.1016/j.exger.2009.02.001.

Kamble P, Selvarajan K, Narasimhulu CA, Nandave M, Parthasarathy S. 2013. Aspirin may promote mitochondrial biogenesis via the production of hydrogen peroxide and the induction of Sirtuin1/PGC-1α genes. *European Journal of Pharmacology* **699**:55–61 DOI 10.1016/j.ejphar.2012.11.051.

Korde AS, Pettigrew LC, Craddock SD, Maragos WF. 2005. The mitochondrial uncoupler 2,4-dinitrophenol attenuates tissue damage and improves mitochondrial homeostasis following transient focal cerebral ischemia. *Journal of Neurochemistry* **94**:1676–1684 DOI 10.1111/j.1471-4159.2005.03328.x.

Koubova J, Guarente L. 2005. How does calorie restriction work? *Genes and Development* **17**:313–321 DOI 10.1101/gad.1052903.

Lanza IR, Nair KS. 2010. Mitochondrial function as a determinant of life span. *Pflügers Archiv - European Journal of Physiology* **459**:277–289 DOI 10.1007/s00424-009-0724-5.

Lee WJ, Kim M, Park H-S, Kim HS, Jeon MJ, Oh KS, Koh EH, Won JC, Kim M-S, Oh GT, Yoon M, Lee K-U, Park J-Y. 2006. AMPK activation increases fatty acid oxidation in skeletal muscle by activating PPAR alpha and PGC-1. *Biochemical and Biophysical Research Communications* **340**:291–295 DOI 10.1016/j.bbrc.2005.12.011.

Lemere BD, Behrendt M, DeCorby A, Gaskova D. 2009. *C. elegans* longevity pathways converge to decrease mitochondrial membrane potential. *Mechanisms of Ageing and Development* **130**:461–465 DOI 10.1016/j.mad.2009.05.001.

Levine YC, Li GK, Michel T. 2007. Agonist-modulated regulation of AMP-activated protein kinase in endothelial cells: evidence for an AMPK→ RAC1→ AKT→ eNOS pathway. *Journal of Biological Chemistry* **282**:20351–20364 DOI 10.1074/jbc.M702182200.

Li F, Zhang L, Craddock J, Bruce-Keller AJ, Dasuri K, Nguyen A, Keller JN. 2008. Aging and dietary restriction effects on ubiquitination, sumoylation, and the proteasome in the heart. *Mechanisms of Ageing and Development* **129**:515–521 DOI 10.1016/j.mad.2008.04.007.

Longo VD, Fontana L. 2010. Calorie restriction and cancer prevention: metabolic and molecular mechanisms. *Trends in Pharmacological Sciences* **31**:89–98 DOI 10.1016/j.tips.2009.11.004.

López-Lluch G, Hunt N, Jones B, Zhu M, Jamieson H, Hilmer S, Cascajo MV, Allard J, Ingram DK, Navas P, de Cabo R. 2006. Calorie restriction induces mitochondrial biogenesis and bioenergetic efficiency. *Proceedings of the National Academy of Sciences of the United States of America* **103**:1768–1773 DOI 10.1073/pnas.0510452103.

Martin-Montalvo A, Mercken EM, Mitchell SJ, Palacios HH, Mote PL, Scheibye-Knudsen M, Gomes AP, Ward TM, Minor RK, Blouin MJ, Schwab M, Pollak M, Zhang Y, Yu Y, Becker KG, Bohr VA, Ingram DK, Sinclair DA, Wolf NS, Spindler SR, Bernier M, de Cabo R. 2013. Metformin improves healthspan and lifespan in mice. *Nature Communications* **4**:Article 2192 DOI 10.1038/ncomms3192.

Mason MG, Nicholls P, Wilson MT, Cooper CE. 2006. Nitric oxide inhibition of respiration involves both competitive (heme) and noncompetitive (copper) binding to cytochrome c oxidase. *Proceedings of the National Academy of Sciences of the United States of America* **103**:708–713 DOI 10.1073/pnas.0506562103.

Mesquita A, Weinberger M, Silva A, Sampaio-Marques B, Almeida B, Leao C, Costa V, Rodrigues F, Burhans WC, Ludovico P. 2010. Calorie restriction or catalase inactivation extends yeast chronological lifespan by inducing H_2O_2 and superoxide dismutase activity. *Proceedings of the National Academy of Sciences of the United States of America* **107**:15123–15128 DOI 10.1073/pnas.1004432107.

Nisoli E, Clementi E, Paolucci C, Cozzi V, Tonello C, Sciorati C, Bracale R, Valerio A, Francolini M, Moncada S, Moncada S, Carruba MO. 2003. Mitochondrial biogenesis in mammals: the role of endogenous nitric oxide. *Science* **299**:896–899 DOI 10.1126/science.1079368.

Nisoli E, Tonello C, Cardile A, Cozzi V, Bracale R, Tedesco L, Falcone S, Valerio A, Cantoni O, Clementi E, Carruba MO. 2005. Calorie restriction promotes mitochondrial biogenesis by inducing the expression of eNOS. *Science* **310**:314–317 DOI 10.1126/science.1117728.

Ou ZJ, Wei W, Huang DD, Luo W, Luo D, Wang ZP, Zhang X, Ou JS. 2010. L-Arginine restores endothelial nitric oxide synthase-coupled activity and attenuates monocrotaline-induced pulmonary artery hypertension in rats. *American Journal of Physiology, Endocrinology and Metabolism* **298**:E1131–E1139 DOI 10.1152/ajpendo.00107.2010.

Qiu X, Brown K, Hirschey MD, Verdin E, Chen D. 2010. Calorie restriction reduces oxidative stress by SIRT3-mediated SOD2 activation. *Cell Metabolism* **12**:662–667 DOI 10.1016/j.cmet.2010.11.015.

Ristow M. 2014. Unraveling the truth about antioxidants: mitohormesis explains ROS-induced health benefits. *Nature Medicine* **20**:709–711 DOI 10.1038/nm.3624.

Ristow M, Kim Z. 2010. How increased oxidative stress promotes longevity and metabolic health: the concept of mitochondrial hormesis (mitohormesis). *Experimental Gerontology* **45**:410–418 DOI 10.1016/j.exger.2010.03.014.

Rodgers JT, Lerin C, Haas W, Gygi SP, Spiegelman BM, Puigserver P. 2005. Nutrient control of glucose homeostasis through a complex of PGC-1 alpha and SIRT1. *Nature* **434**:113–118 DOI 10.1038/nature03354.

Spindler SR. 2010. Calorie restriction: from soup to nuts. *Ageing Research Reviews* **9**:324–353 DOI 10.1016/j.arr.2009.10.003.

Vera E, Bernardes de Jesus B, Foronda M, Flores JM, Blasco MA. 2013. Telomerase reverse transcriptase synergizes with calorie restriction to increase health span and extend mouse longevity. *PLoS ONE* **8**:e53760 DOI 10.1371/journal.pone.0053760.

Wang DT, Wu M, Li SM, Gao Q, Zeng QP. 2015. Artemisinin mimics calorie restriction to extend yeast lifespan via a dual-phase mode: a conclusion drawn from global transcriptome profiling. *Science China Life Sciences* **58**:1–15 DOI 10.1007/s11427-014-4795-y.

Wang DT, Zeng QP. 2014. Modulation of yeast transporter gene expression and lipid metabolism by hormesis mimicking calorie restriction. *Microbiol China* **41**:2012–2021 DOI 10.13344/j.microbiol.china.130928.

Wu P, Bao F, Zheng Q, Xiao N, Wang DT, Zeng QP. 2012. Artemisinin and rapamycin compromise nitric oxide-driven and hypoxia-triggered acute articular synovitis in mice. *Scientia Sinica Vitae* **42**:724–738 DOI 10.1360/052012-148.

Xiong J, Fan S, Meng Q, Schramm L, Wang C, Bouzahza B, Zhou J, Zafonte B, Goldberg ID, Haddad BR, Pestell RG, Rosen EM. 2003. BRCA inhibition of telomerase activity in cultured cells. *Molecular and Cellular Biology* **23**:8668–8690 DOI 10.1128/MCB.23.23.8668-8690.2003.

Yang W, Hekimi S. 2010. A mitochondrial superoxide signal triggers increased longevity in *Caenorhabditis elegans*. *PLoS Biology* **8**:e1000556 DOI 10.1371/journal.pbio.1000556.

Zeng QP, Xiao N, Wu P, Yang XQ, Zeng LX, Guo XX, Zhang PZ, Qiu F. 2011. Artesunate potentiates antibiotics by inactivating bacterial heme-harbouring nitric oxide synthase and catalase. *BMC Research Notes* **4**:223 DOI 10.1186/1756-0500-4-223.

Zeng QP, Zhang PZ. 2011. Artesunate mitigates proliferation of tumor cells by alkylating heme-harboring nitric oxide synthase. *Nitric Oxide* **24**:110–112 DOI 10.1016/j.niox.2010.12.005.

Zhang S, Gerhard GS. 2009. Heme mediates cytotoxicity from artemisinin and serves as a general anti-proliferation target. *PLoS ONE* **4**:e7472 DOI 10.1371/journal.pone.0007472.

Zhao KC, Xuan WY, Zhao Y, Song ZY. 1989. The pharmacokinetics of a transdermal preparation of artesunate in mice and rabbits. *Yao Xue Xue Bao* **24**:813–816.